Scientific Research Publishing

Open Journal of Veterinary Medicine, 2022, 12, 171-186
https://www.scirp.org/journal/ojvm
ISSN Online: 2165-3364
ISSN Print: 2165-3356

Anatomical and Radiological Description of the *Macaca fascicularis* Spine in Comparison with the Human Spine

Anant Krishnan[1,2*], Guneet Kaleka[1], Scott Emerson[2], Guy Sovak[3], Heather Simmons[4], Kevin Brunner[4], Dane Schalk[4], John Sledge[5], Amber Hoggatt[6], Shanker Nesathurai[4,7,8]

[1]Department of Diagnostic Radiology, Oakland University William Beaumont School of Medicine, Auburn Hills, USA
[2]Department of Diagnostic Radiology and Molecular Imaging, Beaumont Hospital, Royal Oak, USA
[3]Canadian Memorial Chiropractic College, Toronto, Canada
[4]Wisconsin National Primate Research Center, Madison, USA
[5]Lafayette Bone and Joint Clinic, Lafayette, USA
[6]Harvard Medical School, Boston, USA
[7]Department of Physical Medicine and Rehabilitation, Hamilton Health Sciences Corporation, Hamilton, Canada
[8]Division of Physical Medicine and Rehabilitation, Michael G. DeGroote School of Medicine, McMaster University, Hamilton, Canada
Email: *Anant.krishnan@beaumont.edu

How to cite this paper: Krishnan, A., Kaleka, G., Emerson, S., Sovak, G., Simmons, H., Brunner, K., Schalk, D., Sledge, J., Hoggatt, A. and Nesathurai, S. (2022) Anatomical and Radiological Description of the *Macaca fascicularis* Spine in Comparison with the Human Spine. *Open Journal of Veterinary Medicine*, **12**, 171-186.
https://doi.org/10.4236/ojvm.2022.1212014

Received: September 28, 2022
Accepted: December 3, 2022
Published: December 6, 2022

Abstract

Background: This paper describes and displays the spinal radiological anatomy and associated pathology in a *Macaca fascicularis* and compares it to the spinal anatomy of humans. Animal models are commonly used in research. As compared to *Macaca mulatta*, the anatomy of *M. fascicularis* is less well described in the literature. Materials and methods: The authors anatomically reconstructed and reviewed the defleshed spine of a single adult *M. fascicularis* visually, radiographically, and with high resolution CT. Results: 7 cervical, 12 thoracic, 6 lumbar, 3 sacral, and 16 caudal vertebrae were identified. Similarities in the spine to humans were seen as well as differences such as the beaked anterior arch of C1, the anterior pointed lower lumbar vertebrae, the upward curved transverse processes, and presence of three sacral segments. Degenerative changes were seen at multiple locations similar to humans though most pronounced at T3-4. Conclusions: This paper addresses the normal spinal anatomy and degenerative changes in an adult *M. fascicularis* and compares it to humans.

Keywords

Macaca Fascicularis, Macaques, Spine Anatomy, Radiology, CT, Comparative Study, Computed Tomography

1. Introduction

Animal models advance the understanding of human pathology, physiology, behavior, and development. These models have an important role in advancing medical knowledge in diverse fields such as veterinary and human imaging, organ and tissue transplant, vaccine development and medical devices [1]. The choice of animal is based on similarity of physiology, neuroanatomy, reproduction, development, cognition and social complexity [2].

Of the vertebrate animal models used in research, 90% are mice, rats and or other rodents [2]. Non-human primates (NHP) are less commonly used, but have an important role. This is due to the genetic, immunologic, physiologic, and endocrine similarities between this species and human beings. *Macaca mulatta* and *Macaca fascicularis* are commonly used in scientific research. *M. fascicularis*, or cynomolgus macaque [3] is the most commonly used species for testing the safety of drugs [1].

M. fascicularis and humans are genetically similar. Genetic mapping studies have demonstrated a 92.83% sequence similarity when comparing the *M. fascicularis* and human genomes [4]. Gene mapping has found 11,446 one-to-one orthologous genes between *M. fascicularis* and humans [5]. Genes corresponding to Alzheimer's disease, epilepsy, schizophrenia, HIV infection and multiple tumors were found to be orthologous [5]. The close genetic relationship between *M. fascicularis* and human beings is indicative of the common ancestral history between the two species. *M. fascicularis* have been extensively used in research in pharmacology, development, physiology, oncology, skeletal pathology, neurology, ophthalmology, plastic surgery, as well as, gene expression [4]-[10].

While the anatomy of the *M. mulatta* has been well described in the literature [11] [12] [13] [14], the anatomy of *M. fascicularis* has received less attention and published information regarding *M. fascicularis* particularly on radiography and CT is lacking. Given the important role that *M. fascicularis* play in biomedical research, this paper aims to fill this gap by describing and displaying the spinal anatomy and associated pathology in a *M. fascicularis* individual and compare it to human spinal anatomy and relevant pathology.

2. Materials and Methods

A cadaveric defleshed and disinfected skeleton of an adult *M. fascicularis*, born in captivity, was obtained from the New England Regional Primate Research Center. The cadaveric skeleton was derived from an animal that was euthanized as a component of a previous scientific protocol. At Beaumont Hospital, Royal Oak, the authors anatomically reconstructed the various portions of the skeleton using principles, similar to the human skeleton. In concert with a radiology physicist, the reconstructed skeleton was then evaluated in a number of ways including visually (**Figure 1**), radiographically (**Figure 2**), and finally utilizing high resolution multidetector Computed Tomography (CT) (**Figures 3-15**). CT, imaging, as a model, enhances the understanding of living tissues in humans and

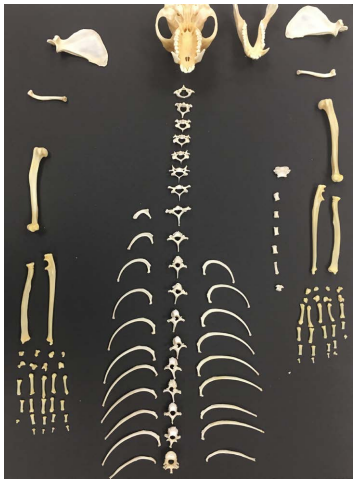

(A)

(B)

Figure 1. Photographs of Skeleton: Surface photographs of the reconstructed skeleton on a cardboard of the *M. fascicularis*. (A) Depicts the seven cervical vertebrae, twelve ribs (on one side, on other side fewer are seen and may have been lost in processing) with associated vertebrae. (B) Depicts the six lumbar vertebrae, sacrum, and caudal segments.

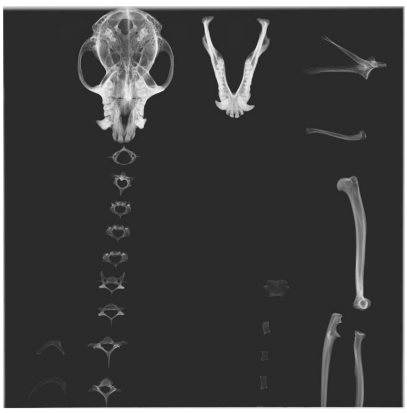

(A)

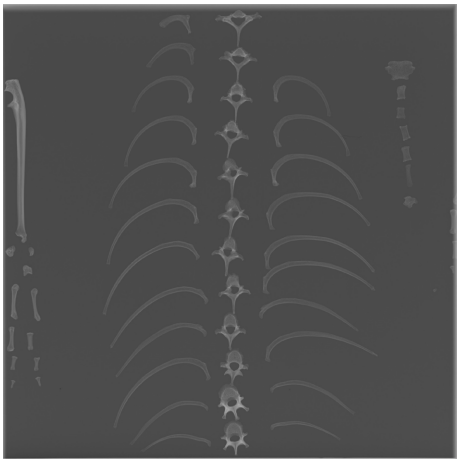

(B)

(C)

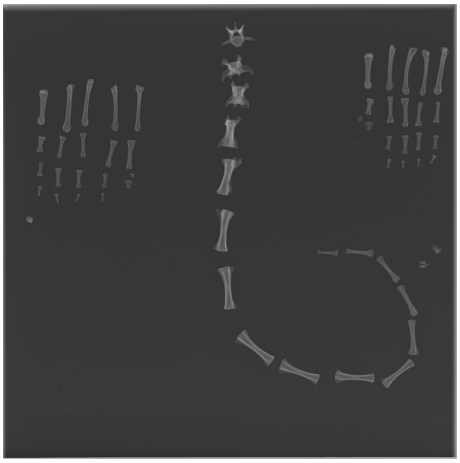

(D)

Figure 2. Radiographs of Skeleton: Radiographs of the skeleton demonstrate the C1 arch, C2 vertebra, and remaining cervical vertebrae (A), thoracic vertebrae (B), lumbar vertebrae and sacrum (C), and caudal vertebrae (D). The skull and rest of skeleton are also included on these radiographs.

Figure 3. CT Topogram of reconstructed skeleton of *M. Fascicularis*. The topogram portrays the various parts of the skeleton laid out on the CT table, from which select vertebrae were reconstructed (on subsequent images). The spine is outlined in the dashed box.

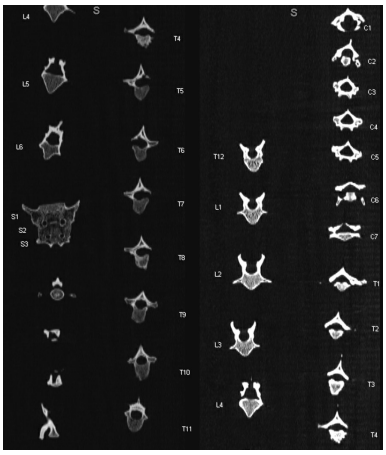

Figure 4. Multiplanar reconstructions of the CT of the *M. fascicularis* spine with labels indicating cervical (C1-C7), thoracic (T1-T12), and lumbar (L1-L6) vertebrae. Caudal vertebrae (proximal 4) are also seen below the sacrum. As a result of scanning without supporting discs or soft tissues, the vertebrae are not precisely aligned in these images.

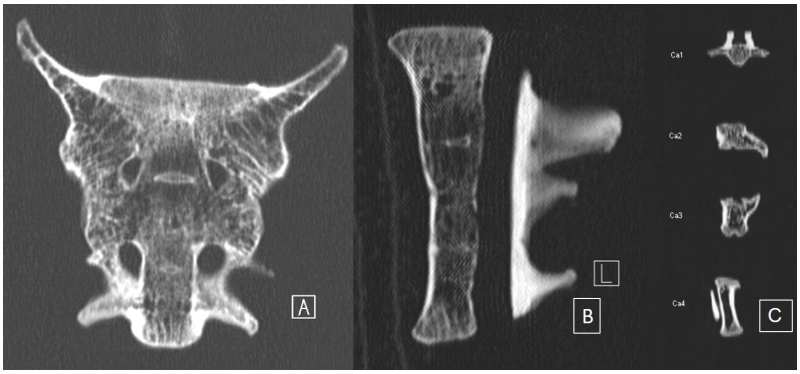

Figure 5. Coronal (A) and Sagittal (B) reconstructed CT images of the sacrum demonstrate three sacral segments and two sacral foramina bilaterally. (C) Image demonstrates the 4 proximal caudal vertebrae of the tail.

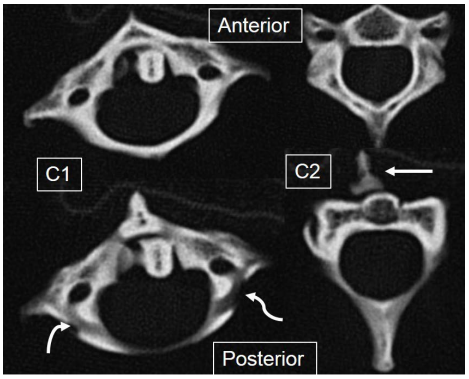

Figure 6. Anatomical reconstructions of the C1 and C2 vertebrae. The C1 to C3 vertebrae were aligned closely together on a wooden framework and then scanned. The expected foramen transversarium and anterior and posterior arches of C1 are remarkably similar to humans. The course of the vertebral arteries over the posterior arch of C1 can be seen (curved arrows). The C2 vertebra is also similar to humans with an odontoid process. A prominent ossific protruberance (straight arrow) arising off the anterior arch of C1 and extending inferiorly is partially captured on the image of the C2 vertebra.

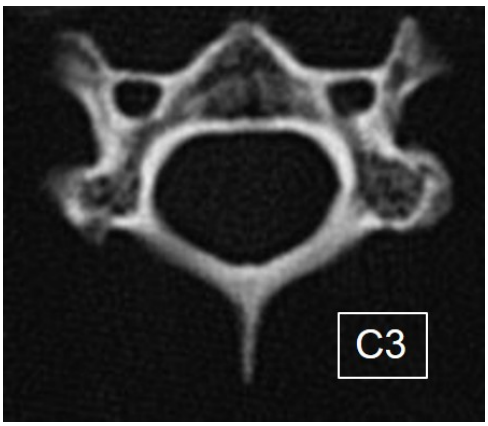

Figure 7. Anatomically realigned axial image of the C3 vertebra demonstrates bilateral foramen transversarium, transverse processes, and posterior spinous process.

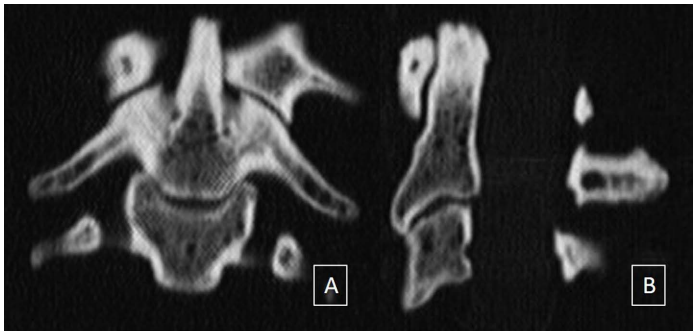

Figure 8. (A) and (B) are coronal and sagittal reconstructions respectively of the C1-3 vertebrae performed on a wooden construct. The gentle downsloping transverse processes of C2 can be seen on image A. The lateral masses of C1 and C2 are asymmetrically profiled as a result of rotation of C1 on C2.

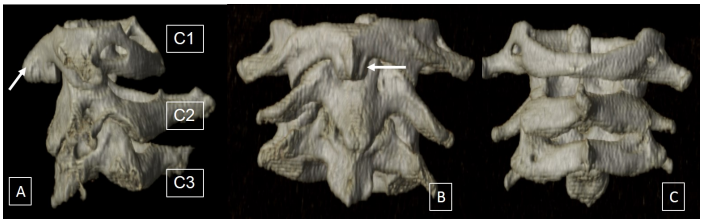

Figure 9. (A), (B), and (C) are 3D volumetric reconstructions of the C1 - C3 vertebrae with a sideways profile on A, anterior view on B, and posterior view on C. C1 to C3 are labelled. Note again the prominent ossific protruberance (arrows) off the C1 anterior arch, best profiled on A, but also seen on B.

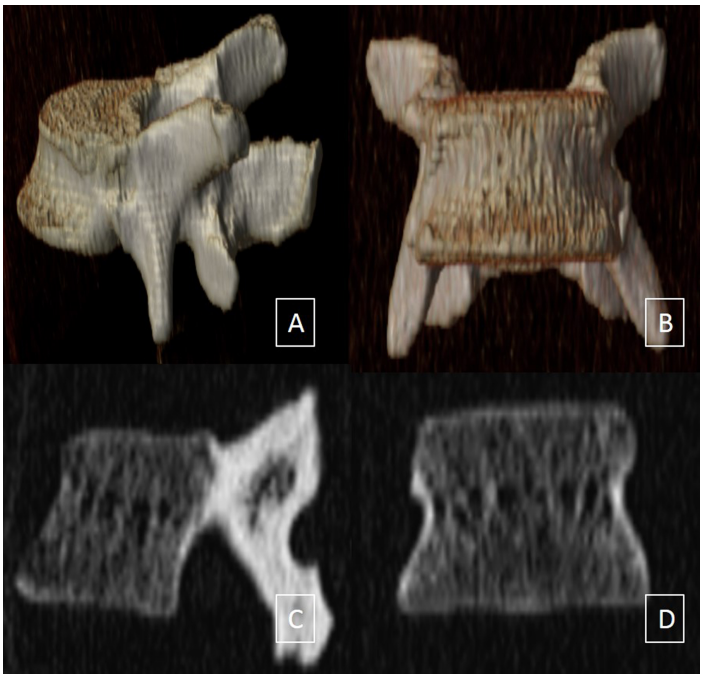

Figure 10. Example of a thoracic vertebra. 3D volume rendered (A) Lateral oblique and (B) Frontal Projections) and Sagittal (C) and Coronal (D) CT reconstructions of the T11 vertebra.

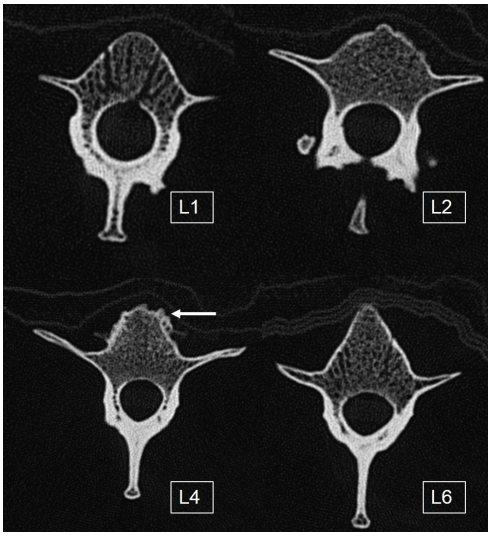

Figure 11. Lumbar vertebrae examples. Axial reconstructed CT images of the L1, L2, L4, and L6 vertebrae. As can be seen there is progressive alteration in the shape of the vertebral bodies with the lower vertebral bodies revealing a pointed anterior body. The transverse processes in the lower lumbar vertebrae are longer and curve cranially. Degenerative changes including spurring is seen along the anterior aspect of the L4 vertebral body (arrow).

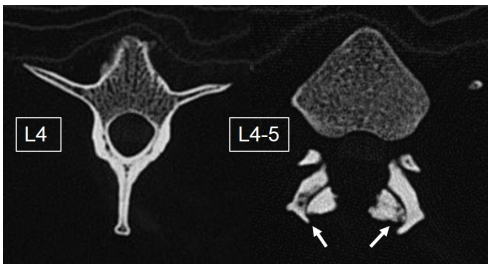

Figure 12. L4 vertebra and L4-5 foramen. In addition to degenerative spurring along the anterior aspect of L4, facet arthropathy (arrows) is also seen at L4-5 with bony overgrowth and subchondral lucencies.

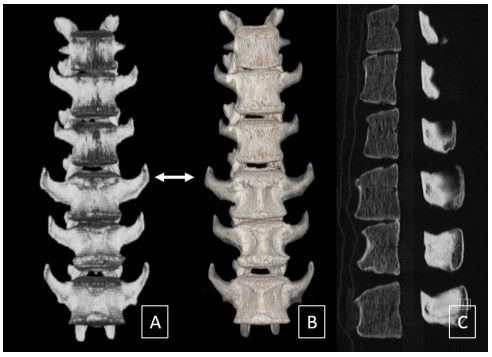

Figure 13. Surface shaded (A), 3D volume rendered (B), and sagittal mid body reconstruction (C) of the six lumbar vertebrae performed over a wooden construct. Progressive increase in size and prominence of the transverse processes from L1 caudally is seen. The most prominent in our specimen was at L4. The upward curvature of the transverse processes in the lumbar vertebrae mimic "Viking horns" (arrow).

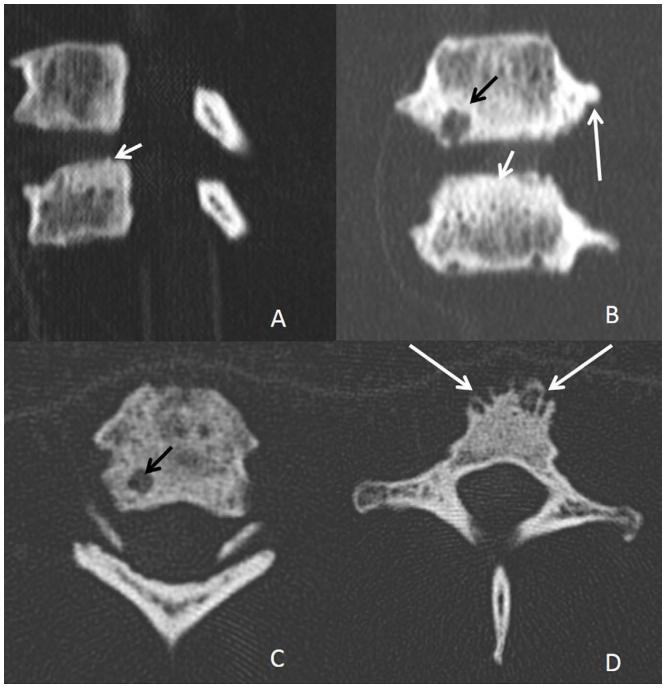

Figure 14. CT scans of T3 and T4 vertebrae reassembled to mimic normal alignment. Sagittal (A), coronal (B), and axial (C, D) reconstructed images of the T3, T4 vertebrae demonstrate degenerative changes including endplate sclerosis (short white arrows in A and B), subchondral cyst at the inferior endplate of T3 (black arrows in B and C) and osteophytosis (long white arrows in B and D).

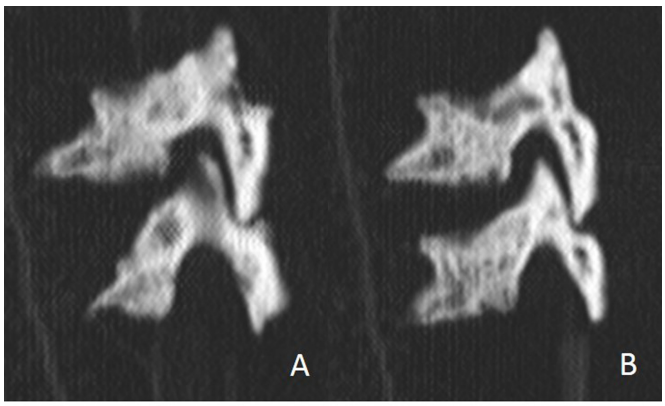

Figure 15. CT scans of T3 and T4 vertebrae reassembled to mimic normal alignment. Parasagittal images of the facets reveal some degenerative changes on one side (A) and minimal to none on the other side (B).

animals as well as cadaveric tissues. CT scans were taken using an ultra high resolution (UHR) protocol on a Siemens Definition Flash scanner (Erlangen, Germany). The UHR images were acquired using a 16 × 0.3 mm beam, 120 kVp, 225 effective mAs, and a pitch = 1. Images were reconstructed with a thickness of 2 mm using the U75u algorithm and a 140 mm field of view (300 mm scan field of view). Digital radiographs were taken on a GE Definium 8000 (General Electric

Healthcare, Chicago, IL). Images were acquired with a 50 kVp and 2 mAs setting, using the small focal spot. Images were acquired using the "Hand" protocol for basic bone enhancement. Since there was no soft tissue, the technique was lowered. CT images were reviewed on a PACS (picture archiving and communication system) station. As the specimen lacked soft tissue (such as intervertebral discs) to closely align the vertebrae, additional reconstructions of select vertebrae was performed in order to mimic the alignment of vertebrae in the spine. This was accomplished using Balsa wood and tape (chosen to reduce CT artifacts but supportive of the vertebrae). These vertebrae were also scanned on the CT scanner, and axial, coronal, sagittal, and select 3D reconstructions were obtained to better facilitate assessment.

3. Results

3.1. Overview and Cervical Spine

The *M. fascicularis* skeleton depicts many similarities to the human skeleton. The spine of the *M. fascicularis* in particular shares many commonalities with the human spine. The *M. fascicularis* spine has seven cervical vertebrae (**Figures 6-9**). The vertebrae include spinous processes, transverse processes and bodies similar to human vertebrae. Additionally, the vertebrae also depict vertebral arches created by laminas and pedicles as found in humans. The C1 vertebra lacks a vertebral body, similar to the human C1, while the other cervical vertebrae have small bodies. Grooves for the vertebral arteries were seen over the superior surface of the C1 vertebra posteriorly (**Figure 6**). The anterior arch of C1 in our specimen demonstrated in contrast to humans a protuberance (**Figure 6**, **Figure 9**) that has a beaklike appearance (triangular on the transverse images) with a flattened inferior surface on the sagittal images. The C2 vertebra demonstrates a structure similar to the odontoid process found in humans with a similar articulation with C1. Some arthritic changes were seen near the median C1-2 articulation (**Figure 8**). The transverse processes of the C2 and C3 vertebrae were well defined, longer than in humans, but similar to humans angled caudally. Foramen transversarium for the vertebral arteries were found in the transverse processes of the *M. fascicularis* C1-C6 vertebrae as is seen in the human body. Of slight difference from human cervical vertebrae, the C6 vertebra lacks a bifid spinous process. The C7 vertebra, in our specimen, demonstrated the longest spinous process, but only slightly greater than C6, in contrast to the typically prominent spinous process of C7 in humans known as vertebra prominens.

3.2. Thoracic Spine

Our specimen depicts twelve rib bearing thoracic vertebrae. Of note, 12 ribs were seen on the right side and 10 were seen on the left side; this may be due to anatomical asymmetry of the number of ribs and/or loss during processing. The upper thoracic vertebrae demonstrate somewhat small and horizontal transverse processes. The lower thoracic vertebrae, for example T11 (**Figure 10**), demon-

strate somewhat slender and inferiorly directed transverse processes. The vertebral body is also more rounded with a circular spinal canal. The first thoracic vertebra has a long spinous process. Additionally, the spinous processes of the thoracic vertebrae are long and slope postero-inferiorly. These properties of the *M. fascicularis* thoracic vertebrae are similar to characteristics found in the human thoracic vertebrae. The last two thoracic vertebrae were the largest.

3.3. Lumbar Spine

This specimen depicted six non rib bearing lumbar vertebrae (**Figures 11-13**). These vertebrae depict larger bodies as compared with the thoracic and cervical vertebrae. The upper lumbar vertebrae show some features similar to the lower thoracic vertebrae though with small transversely oriented transverse processes. Progressively, the transverse processes in the lumbar vertebrae become longer and curve superiorly, particularly prominent at L4 through L6 in our specimen. This appearance, to us, mimics the horns of a "Viking Helmet" (**Figure 13**). Similar to the lumbar vertebrae found in humans, the *M. fascicularis* lumbar vertebrae have a large spinal canal, and short spinous processes. Additionally while the upper lumbar vertebrae have a relatively reniform vertebral body, the lower lumbar vertebrae have a more beak like appearance anteriorly. This is distinct and different from those in humans.

3.4. Sacrum and Caudal Segments

The sacrum depicts structures analogous to the sacral promontory, and median sacral crest found in the human sacrum. As opposed to the human sacrum, which is composed of five fused sacral segments and 4 sacral foramina, the *M. fascicularis* specimen depicts three fused sacral segments and two sacral foramina (**Figure 5**). We identified a total of 16 caudal vertebrae and a few tiny ossific fragments, which we believe make up the tail of the *M. fascicularis*. Caudal vertebrae in primates are described as being made of three parts, the proximal, transition, and distal. The first 4 segments constitute the proximal caudal vertebrae. Of these, the first three demonstrate a neural arch, with downsloping and well developed transverse processes and superior and inferior facet joints. The transition vertebra which is part of the proximal demonstrates an arch, but has facet joints only superiorly. The next two are the transitional vertebra that lack a neural arch but have articulations. The second of these is the longest vertebra. The remaining vertebrae progressively decrease in size and are the distal caudal segments of which we were able to identify 10. These distal caudal segments on cross sectional imaging, depicted a groove at one end and 4 ridge like protuberances, probably representing the two small transverse processes and the bifid spinous process.

3.5. Pathological Findings

The vertebrae of this specimen also demonstrates degenerative or senescent

changes similar to those seen in humans. Some of the vertebral bodies depict loss of height, endplate sclerosis, and osteophytosis. In our sample, degenerative changes were best seen at the C1-2, C7, T2, T3, T4, T8, and L4 levels with most pronounced findings at T3-T4 (**Figure 14**, **Figure 15**). Sclerosis was seen along the adjoining endplates of T4 and T3. A focus of subchondral cyst formation along the inferior endplate of T3 was also seen along with the osteophytes. These changes are reminiscent of osteoarthritic changes noted in humans with spinal disk degeneration. The disks could not be evaluated as we reviewed only the osseous elements.

4. Discussion

The *M. fascicularis* specimen described had seven cervical vertebrae, twelve rib-bearing thoracic vertebrae, and six lumbar vertebrae. Human beings typically have 5 lumbar vertebrae, although this is subject to some anatomical variation. In humans, numbering of vertebrae is essential before surgery to perform procedural treatment at the correct level (for example in spinal fusion with instrumentation, facet joint injections, etc.) [15]. Often, whole spine radiographs or in the case of MRI, cervico-thoracic localizers are used to accurately number the spine from C2 caudally. The first 7 vertebrae are labeled as cervical, as the cervical spine demonstrates morphological stasis [16] [17]. Typically, radiologists number the next rib bearing vertebrae as thoracic; this is typically 12, but there is some variability, with some as many as 13, based on the presence of the extra singular or paired rib(s). Of note, humans also occasionally demonstrate a pair of cervical ribs but these are not usually confused given their location articulating with the C7 vertebrae.

Following the thoracic vertebrae, the next non-rib bearing vertebrae, by convention, are referred to as lumbar vertebrae. In this *M. fascicularis* specimen, we identified twelve thoracic and six lumbar vertebrae. In related research (personal communication by author SN), we have noted that some *M. fascicularis* subjects have 7 lumbar vertebrae.

While human beings typically have five lumbar vertebrae, numerical variants, as well as, lumbosacral transitional vertebrae (LSTV) are common. The prevalence of LSTV is approximately 30% of the general population; this is often associated with numerical variants in the number of lumbar vertebrae [18]. An understanding of the evolution and presence of LTSV and numerical variants in humans through research in NHP would be illuminating; these anatomical variations, in human medicine, have been contributors to errors in procedural and surgical treatments [16]. Transitional vertebrae have also been associated with early degeneration of intervertebral discs above the transitional vertebrae. This phenomenon is associated with altered biomechanics [19] and low back pain (Bertolotti syndrome). This is a disorder that affects young people and is refractory to medications and as well interventional pain treatment [20] [21].

Additionally, numerical variants and LSTV have been found to be associated

with dermatomal variation and an alteration in nerve function [4].

Osteoarthritic changes commonly seen in the human spine on imaging were also observed in our specimen. As has been described in the literature [22], disc pathology is different according to the site in spine. It is well described in humans in the cervical spine with endplate sclerosis, and osteophyte formation [22] [23]. Thoracic disease is less common than cervical or lumbar disease [22]. Rhesus macaques show more prominent age related kyphosis in the lower thoracic spine with osteophyte formation especially along the anterior aspect of the vertebrae, in contrast to humans [24] [25]. The *M. fascicularis* is interesting in that it sometimes assumes an erect position similar to humans [22]. In our specimen, the most pronounced degenerative changes were at T3-4. This is also the level that is believed to have the smallest disc space [22]. This osteoarthritic process lends NHP models to research, addressing interventions for degenerative disease. Current treatment in humans with degenerative spine conditions diseases consist primarily of combination of lifestyle changes, physical interventions, pharmacologic pain relief, as well as procedural and surgical treatment; the long term efficacy of these treatments is subject to significant controversy. While these interventions provide some relief to patients, they do not completely address the underlying pathophysiology.

The *M. fascicularis* is a particularly appropriate candidate for studies in degenerative bone diseases not only due to similar anatomy, as noted in this study, but also due to similarity in bone structure itself. Among various animals including rabbits, dog, and non human primates studied by microcomputed tomography and radiology, *M. fascicularis* bone structure, density and microanatomy were most similar to that of humans, making them the most desirable species to conduct preclinical research [26]. This is also helpful in orthopedic research in the spine and knee. Importantly, following open knee surgeries and knee joint cartilage sampling, *M. fascicularis* have been demonstrated to be appropriate models for age-related knee osteoarthritis [6]. Anatomical findings that made *M. fascicularis* an appropriate model for knee osteoarthritis may also make it a fit for studies into degenerative diseases overall.

The tail of the *M. fascicularis* also presents further opportunities for discovery. This species has a particularly long tail with twenty-six vertebrae with a variation of three to six vertebrae [27]. Consistent with descriptions in the literature [27], the first 4 had a neural arch and are referred to as proximal, including the transition vertebra, followed by the two transitional and long vertebrae and finally the distal caudal vertebrae. It is possible that in processing a few caudal fragments were lost as we identified a total of 16 caudal segments in our specimen. Alternatively, there may be biological variability accounting for the difference between our specimen and literature. The tail is supplied by 4 long nerves that have motor neuron pools in the spinal cord. The length of the tail can yield information regarding peripheral nerve pathology and possible treatments [28] [29]. Tail length variations amongst macaque species, have an evolutionary basis; it is con-

sidered an adaptive mechanism for thermoregulation and balance during locomotion [27]. These longer tail lengths lend themselves to the need for a more developed peripheral nervous system, with the existence of longer neurons for control of the tail. In turn, these longer neurons of the long tailed *M. fascicularis* as compared to the short tailed *M. mulatta* can better facilitate nerve conduction and similar studies in research.

5. Limitations

This study is based on a single skeleton. There is biological heterogeneity related to the anatomic structures in animals as with humans. However, to our knowledge, this is the only CT assessment of the skeleton of the M. fascicularis, which we hope will stimulate better understanding of these animals.

6. Conclusion

This paper addressed the skeletal structure of the spine, of a *M. fascicularis* specimen with an effort to describe both normal anatomy, and degenerative changes. These findings can be extrapolated to other parts of the skeletal system to facilitate further orthopedic, skeletal and neurology research. The similarities in the skeletal structure and genetic identities of *M. fascicularis* and humans suggests that using this NHP species as a model can provide invaluable information regarding human pathologies and possible treatments. This paper has the limitation of analyzing a single individual *M. fascicularis*. Without other specimens, it is difficult to draw conclusions regarding the skeletal structures of *M. fascicularis* as a species. Despite these limitations, this description provides insight into the skeletal structure of the spine of *M. fascicularis* and suggests future directions of research.

Location of Study

Anatomical reconstruction of skeleton bones and scanning was done at Beaumont Hospital, Royal Oak (described also in materials and methods).

Conflicts of Interest

The authors declare no conflicts of interest regarding the publication of this paper.

References

[1] Lankau, E.W., Turner, P.V., Mullan, R.J. and Galland, G.G. (2014) Use of Nonhuman Primates in Research in North America. *Journal of the American Association for Laboratory Animal Science*: *JAALAS*, **53**, 278-282.

[2] Phillips, K.A., Bales, K.L., Capitanio, J.P., *et al.* (2014) Why Primate Models Matter. *American Journal of Primatology*, **76**, 801-827. https://doi.org/10.1002/ajp.22281

[3] Ong, P. and Richardson, M. (2020) *Macaca fascicularis*.

[4] Ebeling, M., Kung, E., See, A., *et al.* (2011) Genome-Based Analysis of the Nonhu-

man Primate *Macaca fascicularis* as a Model for Drug Safety Assessment. *Genome Research*, **21**, 1746-1756. https://doi.org/10.1101/gr.123117.111

[5] Tan, T., Xia, L., Tu, K., *et al.* (2018) Improved *Macaca fascicularis* Gene Annotation Reveals Evolution of Gene Expression Profiles in Multiple Tissues. *BMC Genomics*, **19**, Article No. 787. https://doi.org/10.1186/s12864-018-5183-y

[6] Liu, G., Zhang, L., Zhou, X., *et al.* (2018) Selection and Investigation of a Primate Model of Spontaneous Degenerative Knee Osteoarthritis, the Cynomolgus Monkey (*Macaca fascicularis*). *Medical Science Monitor*: *International Medical Journal of Experimental and Clinical Research*, **24**, 4516-4527. https://doi.org/10.12659/MSM.908913

[7] Shidahara, Y., Natsume, T., Awaga, Y., *et al.* (2019) Distinguishing Analgesic Drugs from Non-Analgesic Drugs Based on Brain Activation in Macaques with Oxaliplatin-Induced Neuropathic Pain. *Neuropharmacology*, **149**, 204-211. https://doi.org/10.1016/j.neuropharm.2019.02.031

[8] Placi, S., Eckert, J., Rakoczy, H. and Fischer, J. (2018) Long-Tailed Macaques (*Macaca fascicularis*) Can Use Simple Heuristics but Fail at Drawing Statistical Inferences from Populations to Samples. *Royal Society Open Science*, **5**, Article ID: 181025. https://doi.org/10.1098/rsos.181025

[9] Kaltreider, S.A., Wallow, I.H., Gonnering, R.S. and Dortzbach, R.K. (1987) The Anatomy and Histology of the Anophthalmic Socket—Is the Myofibroblast Present? *Ophthalmic Plastic & Reconstructive Surgery*, **3**, 207-230. https://doi.org/10.1097/00002341-198703040-00001

[10] Jr., J.M.M., Faulkner, J.A. and Cote, C. (1989) Transplantation and Transposition of Skeletal Muscles into the Faces of Monkeys. *Plastic and Reconstructive Surgery*, **84**, 424-423. https://doi.org/10.1097/00006534-198909000-00007

[11] Fridman, Ė.P. and Nadler, R.D. (2002) Medical Primatology: History, Biological Foundations and Applications. Taylor & Francis, London.

[12] (1934) Anatomy of the Primates. The Anatomy of the Rhesus Monkey (*Macaca mulatta*). *Journal of Anatomy*, **68**, 574-575. https://www.ncbi.nlm.nih.gov/pmc/articles/PMC1249015

[13] Hartman, C.G. (1961) The Anatomy of the Rhesus Monkey. Hafner Publication Co., New York.

[14] Chung, B.S., Jeon, C.Y., Huh, J.W., *et al.* (2019) Rise of the Visible Monkey: Sectioned Images of Rhesus Monkey. *Journal of Korean Medical Science*, **34**, e66. https://doi.org/10.3346/jkms.2019.34.e66

[15] Konin, G.P. and Walz, D.M. (2010) Lumbosacral Transitional Vertebrae: Classification, Imaging Findings, and Clinical Relevance. *AJNR. American Journal of Neuroradiology*, **31**, 1778-1786. https://doi.org/10.3174/ajnr.A2036

[16] Carrino, J.A., Jr., P.D.C., Lin, D.C., *et al.* (2011) Effect of Spinal Segment Variants on Numbering Vertebral Levels at Lumbar MR Imaging. *Radiology*, **259**, 196-202. https://doi.org/10.1148/radiol.11081511

[17] Galis, F. (1999) Why Do Almost All Mammals Have Seven Cervical Vertebrae? Developmental Constraints, Hox Genes, and Cancer. *Journal of Experimental Zoology*, **285**, 19-26. https://doi.org/10.1002/(SICI)1097-010X(19990415)285:1<19::AID-JEZ3>3.0.CO;2-Z

[18] Furman, M.B., Wahlberg, B. and Cruz, E.J. (2018) Lumbosacral Transitional Segments: An Interventional Spine Specialist's Practical Approach. *Physical Medicine and Rehabilitation Clinics of North America*, **29**, 35-48. https://doi.org/10.1016/j.pmr.2017.08.004

[19] Holm, E.K., Bunger, C. and Foldager, C.B. (2017) Symptomatic Lumbosacral Transitional Vertebra: A Review of the Current Literature and Clinical Outcomes Following Steroid Injection or Surgical Intervention. *SICOT-J*, **3**, Article No. 71. https://doi.org/10.1051/sicotj/2017055

[20] Jain, A., Agarwal, A., Jain, S. and Shamshery, C. (2013) Bertolotti Syndrome: A Diagnostic and Management Dilemma for Pain Physicians. *The Korean Journal of Pain*, **26**, 368-373. https://doi.org/10.3344/kjp.2013.26.4.368

[21] Shaikh, A., Khan, S.A., Hussain, M., *et al.* (2017) Prevalence of Lumbosacral Transitional Vertebra in Individuals with Low Back Pain: Evaluation Using Plain Radiography and Magnetic Resonance Imaging. *Asian Spine Journal*, **11**, 892-897. https://doi.org/10.4184/asj.2017.11.6.892

[22] Longo, U.G., Ripalda, P., Denaro, V. and Forriol, F. (2006) Morphologic Comparison of Cervical, Thoracic, Lumbar Intervertebral Discs of Cynomolgus Monkey (*Macaca fascicularis*). *European Spine Journal*: *Official Publication of the European Spine Society, the European Spinal Deformity Society, and the European Section of the Cervical Spine Research Society*, **15**, 1845-1851. https://doi.org/10.1007/s00586-005-0035-2

[23] Prescher, A. (1998) Anatomy and Pathology of the Aging Spine. *European Journal of Radiology*, **27**, 181-195. https://doi.org/10.1016/S0720-048X(97)00165-4

[24] Bailey, J.F., Fields, A.J., Liebenberg, E., Mattison, J.A., Lotz, J.C. and Kramer, P.A. (2014) Comparison of Vertebral and Intervertebral Disc Lesions in Aging Humans and Rhesus Monkeys. *Osteoarthritis and Cartilage*, **22**, 980-985. https://doi.org/10.1016/j.joca.2014.04.027

[25] Simmons, H.A. (2016) Age-Associated Pathology in Rhesus Macaques (Macaca mulatta). *Veterinary Pathology*, **53**, 399-416. https://doi.org/10.1177/0300985815620628

[26] Bagi, C.M., Berryman, E. and Moalli, M.R. (2011) Comparative Bone Anatomy of Commonly Used Laboratory Animals: Implications for Drug Discovery. *Comparative Medicine*, **61**, 76-85.

[27] Wakamori, H. and Hamada, Y. (2019) Skeletal Determinants of Tail Length Are Different between Macaque Species Groups. *Scientific Reports*, **9**, Article No. 1289. https://doi.org/10.1038/s41598-018-37963-z

[28] Seth, N., Simmons, H.A., Masood, F., *et al.* (2018) Model of Traumatic Spinal Cord Injury for Evaluating Pharmacologic Treatments in Cynomolgus Macaques (*Macaca fasicularis*). *Comparative Medicine*, **68**, 63-73. https://doi.org/10.4236/ojvm.2013.31014

[29] Graham, W.A., Rosene, D.L., Westmoreland, S., Miller, A., Sejdic, E. and Nesathural, S. (2013) Humane Non-Human Primate Model of Traumatic Spinal Cord Injury Utilizing Electromyography as a Measure of Impairment and Recovery. *Open Journal of Veterinary Medicine*, **3**, 86-89.